

The scaling relation of early-type galaxies in clusters. II: Spectroscopic data for galaxies in eight nearby clusters*

D. Bettoni¹, M. Moles², P. Kjørgaard³, G. Fasano¹, and J. Varela¹

¹ Osservatorio Astronomico di Padova, Vicolo de' ll Osservatorio 5, I-35122 Padova
e-mail: bettoni@pd.astro.it, fasano@pd.astro.it, varela@pd.astro.it

² Instituto de Astrofísica de Andalucía, Consejo Superior de Investigaciones Científicas, Camino Bajo de Huétor 50, Apdo. 3004, 18080 Granada, Spain
e-mail: moles@iaa.es

³ Copenhagen University Observatory. The Niels Bohr Institute for Astronomy, Physics and Geophysics, Juliane Maries Vej 30, DK-2100 Copenhagen
e-mail: per@astro.ku.dk

Received

ABSTRACT

Aims. We present in this work low and intermediate resolution spectroscopic data collected for 152 early type galaxies in 8 nearby clusters with $z \leq 0.10$.

Methods. We use low resolution data to produce the redshift and the K-correction for every individual galaxy, as well as to give their overall spectral energy distribution, and some spectral indicators, including the 4000Å break, the Mg₂ strength, and the NaD equivalent width. We have also obtained higher resolution data for early type galaxies in three of the clusters, to determine their central velocity dispersion.

Results. The effect of the resolution on the measured parameters is discussed.

Conclusions. New accurate systemic redshift and velocity dispersion is presented for four of the surveyed clusters, A98, A3125, A3330, and DC2103-39. We have found that the K-correction values for E/S0 bright galaxies in a given nearby clusters are very similar. We also find that the distribution of the line indicators significantly differ from cluster to cluster.

Key words. Galaxies:elliptical and lenticulars – redshifts – clusters,general

1. Introduction

This is the second paper to present data on nearby clusters of galaxies. The motivations and details of the program have been given in Fasano et al (2002, hereafter Paper I; see also Fasano et al 2000), following the proposal discussed by Kjørgaard, Jørgensen, and Moles (1993, hereafter KJM; see also Moles et al. 1998). They will be used together with the results from the project WINGS (Fasano et al. 2006) to analyze, among others the scaling relations of early-type galaxies in clusters.

Here we present low resolution (20Å and 40Å, LRS/20 and LRS/40 respectively in the following) and intermediate resolution spectroscopy (3.3 Å resolution, IRS in the following) of 152 early type galaxies in 8 nearby clusters.

Send offprint requests to: D. Bettoni

* Based on data obtained with the Nordic Optical Telescope (La Palma, Spain) with ALFOSC. Also based on observations obtained with DFOSC at the D1.54m telescope at the European Southern Observatory (La Silla, Chile)

The LRS data are intended to provide the redshifts of the candidate galaxies, to establish their membership to a given cluster. They also allow the measurement of the K-correction for each individual galaxy and the strength of some spectral features. Apart from the more often used Mg₂, we consider here two other prominent spectral features, the NaD doublet and the 4000Å break, D4000. The NaD line index is more sensitive to temperature effects than Mg₂, but it can be affected by the presence of interstellar material (Burstein et al 1984; Bica, and Alloin 1986; Bica et al 1991). However, once allowance is made for that, it correlates well with other indices, Mg₂ in particular. Bica, and Alloin (1986) concluded that for a metallicity not greater than solar, any excess of NaD (with respect to the prediction from the Mg₂ indicator) can be due only to interstellar absorption. An outlying position in the Mg₂-NaD plane can therefore be interpreted as a sign of peculiarity (see Bica et al 1991).

The 4000Å break, D4000, is primarily sensitive to the presence of young stars. Hamilton (1985) selected it for

Table 1. Log and setup of the observations

Run	Date	Mode	Tel.	"/pix	Gr. #	λ range(Å)	Å/pix	Res Å ^a
1	Dec/94	LR	D1.54	0.49	4	3300 – 6400	3.9	20
2	Sep/95	LR	D1.54	0.49	4	3300 – 6400	3.9	20
		IR	D1.54	0.49	13	4800 – 5800	0.95	3.3
3	Feb/97	LR	NOT	0.188	7	3800 – 6800	1.5	20
4	Aug/98	LR	NOT	0.188	4	3300 – 6400	3.1	41
5	Aug/99	LR	NOT	0.188	4	3300 – 6400	3.1	41
6	Mar/01	IR	NOT	0.188	13	4800 – 5800	0.5	1.4

^a Resolution corresponds to the 2.5 slit used in all the runs

that reason as a mark to study the evolution of early type galaxies with redshift. Dressler and Shectman (1987) concluded that it is not sensitive to metallicity but only to the presence of young stars, and insisted on the adequacy of the break indicator to follow the cosmic evolution of early type galaxies. On their side, Kimble et al (1989) found that D4000 does correlate with some metallic indicators. The theoretical work by Poggianti and Barbaro (1997) showed that the break is strongly dependent on the effective temperature, and is also sensitive to the metallicity, but only for intermediate temperature stars. On this basis, Barbaro and Poggianti (1997) have developed evolutionary models showing that D4000 would be a measure of the present star formation rate. The calibration of D4000 in terms of the atmospheric stellar parameters is rather complicated as many absorption lines are included in the break. Gorgas et al (1999 and references therein) have made an empirical calibration of the break that can be incorporated into the evolutionary models to predict its value. The most interesting aspect here of the break indicator is its sensitivity to the recent star formation, and therefore its ability to trace evolution.

The intermediate resolution spectroscopy (IRS) data are necessary to determine the central velocity dispersion needed to build the Fundamental Plane. They also provide more accurate spectral line indices, within the covered spectral range. Unfortunately the behavior of the CCDs we used was very noisy at wavelengths shorter than 5200Å. Thus the measurement of the H β and other indices related to rather weak features was uncertain and therefore we do not include them in the present work.

2. Observations and Data Reduction

The observations were carried out during several runs since 1994 with the Danish 1.54m telescope (DKT) at La Silla (Chile), and the Nordic Telescope (NOT) at La Palma (Spain). We used identical focal reducer instruments with both telescopes, DFOSC (DKT) and ALFOSC (NOT), equipped with identical grisms. Some of the data were taken using the MOS possibilities with ALFOSC.

The different runs and instrumental setups are given in Table 1. In all observations we used a 2.5 slit. For the first run the detector was a Thompson 1024×1024 CCD with 19 μ m pixels, whereas we used various thinned Ford-Loral 2024×2024 CCD's with 15 μ m pixels for the other runs.

Template stars, for the measure of radial velocities and the velocity dispersion, of spectral type G8-K3 III, were observed each night as well as nearby galaxies with known and accurate data. These last were used as standard to gauge the accuracy of the calibrations. We also observed several flux standard stars to allow the data to be fully calibrated. Identification and positional information for the cluster galaxies are taken from Dressler (1980). Otherwise we measured the positions on the DSS. In Table 3 in column 1 we give the name (from NED or Simbad databases) in column 2 and 3 the coordinates and finally in column 4 we give the reference identification we used for the spectrum, this identification is that used in Tables 4 and 6 to identify the galaxies for clusters A98 and A3330. The identifications in Tables 4 and 6 for galaxies in the remaining clusters are from Dressler (1980).

The data reduction procedure was similar for the LRS and IRS data. It was performed within IRAF¹ the scientific frames were corrected for bias and flat-field and calibrated using He/Ar arc-lamp. For the MOS data we extracted individual 2D spectra for each object and treated as any other spectra, so we don't refer to them explicitly in the following.

2.1. The Measurement of the Redshift. Internal and external accuracy

Before attempting to measure the redshift of the target galaxies, we checked the accuracy of the zero point in the λ -calibration of every spectrum, examining the position of the night sky line [OI] λ 5577.32 Å. When necessary the spectrum was shifted to that nominal position. For the radial velocity standard stars, given the short exposure time, the night sky lines were not detected so this procedure could not be applied. We decided to put the standards at zero velocity using their own spectral lines; then we used the IRAF cross-correlation package to control the consistency of the method, i. e., that together, they all define a zero velocity system, within the uncertainties.

The standard stars were then used as templates to measure the redshift of the standard galaxies, using the same IRAF packages. The radial velocity was determined as the mean of the results for the different template stars. The typical scatter amounts to 15 km s⁻¹. In all cases the scatter was within the formal uncertainties of the param-

¹ IRAF is the Image Analysis and Reduction Facility made available to the astronomical community by the National Optical Astronomy Observatories, which are operated by the Association of Universities for Research in Astronomy (AURA), Inc., under contract with the U.S. National Science Foundation.

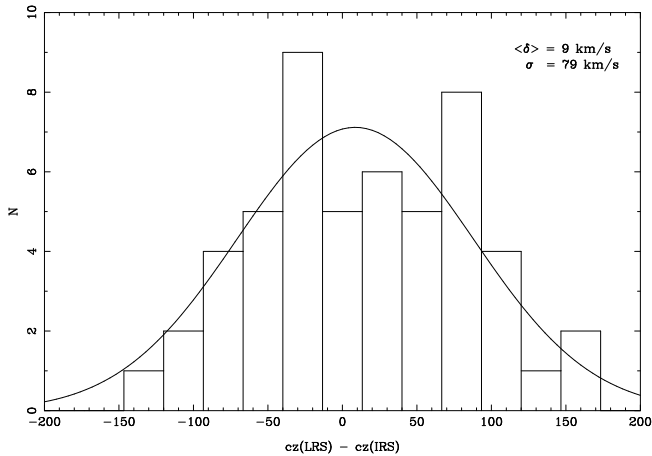


Fig. 1. Distribution of the cz differences for the 52 objects that have both IRS and LRS data. The bin size is 25 km s^{-1} . The solid line is the gaussian fit to the binned data.

eters. The results for those standard galaxies are given in Table 4.

Comparing the results obtained for the standard galaxies from LRS/20 and IRS data (9 cases; there are not galaxies observed in both IRS and LRS/40 modes) we find that the differences in redshift have an average of 7 km s^{-1} , with a scatter of 32 km s^{-1} . Part of that scatter is due to just one galaxy, E462G15, for which the IRS result is 71 km s^{-1} higher than the LRS one. Notice that the IRS value is much closer to the redshift reported by Jørgensen, Franx & Kjaergaard (1996, JFK) for that galaxy.

To check the external consistency of the data we have compared them with other sources, JFK (10 galaxies in common, 7 with IRS data) and Smith et al (2000; 7 objects in common, 5 with IRS data). If we compare only our IRS data, the agreement is excellent with both sources, with $\sigma(\text{diff.}) \sim 15 \text{ km s}^{-1}$. Indeed, the comparison is also good when LRS data are included, except for EG462G15.

Once the consistency of our measured redshift was assured, we decided to use the standard galaxies as templates to determine the redshift of the target cluster galaxies. We found that they give more accurate results than the standard stars, due to the better spectral matching between both sets of galaxies. Each target object was cross-correlated with all the templates. The average of the resulting z values was taken as the redshift of the galaxy, and the scatter as a quality indicator. The heliocentric redshift values are given in Table 4. The code 1 to 4 corresponds to 1σ values of $\leq 50 \text{ km s}^{-1}$, between 50 and 100 km s^{-1} , between 100 and 200 km s^{-1} , and between 200 and 300 km s^{-1} , respectively. That scatter is typically smaller than 75 km s^{-1} , with more than 75% of them within 150 km s^{-1} , even if it reaches up to 300 km s^{-1} in some particular cases.

The internal accuracy of the LRS data can be assessed looking at Figures 1 and 2.

We have searched the literature to examine the external accuracy of our LRS data. The comparison was re-

Table 2. External comparison of the redshift data

Cluster	LRS				IRS		
	Ref.	N	$\Delta(cz)$	σ	N	$\Delta(cz)$	σ
A98	1	10	+36	147	---	---	---
	2	11	-10	120	---	---	---
A119	3	14	+52	75	11	80	48
	4	6	+32	91	6	46	57
	5	5	+3	56	5	28	52
A3125	8	6	-11	121	5	-17	133
A1069	3	7	+29	116	---	---	---
	6	6	+15	162	---	---	---
A1983	7	14	+31	77	---	---	---
A2151	7	9	-15	153	---	---	---

References. 1, Beers et al (1982); 2, Zabludoff et al (1990); 3, Katgert et al (1998); 4, Wegner et al (1999); 5, Huchra et al (1999); 6, Beers et al (1991); 7, Dressler & Shectman (1988); 8, Caldwell, and Rose (1997).

stricted to those sources for which there is a minimum of 5 galaxies in common. The agreement is in general good as can be seen in Table 2. Looking to the actual figures in the table, it would seem that our cz values tend to be slightly greater than most of the others. Whereas this cannot be excluded, the differences are about 50 km s^{-1} or smaller, so we can conclude that our redshift measurements are in the same system as those reported in the quoted references. Indeed, the situation is similar for the IRS data, (see Table 2). The cases for which the disagreement is higher and cannot be accounted for by mere observational errors have been flagged in Table 4, and commented in the footnotes.

2.2. The Measurement of the central velocity dispersion

The velocity dispersion of each target galaxy was determined as the mean of the results for the different template stars. The typical scatter is 10 km s^{-1} . In all cases the scatter was within the formal uncertainties of the parameters. The velocity dispersion and the radial velocity were derived, both for the comparison galaxies and for the target galaxies, with the Fourier Quotient Technique (Sargent et al 1977; Bertola et al 1984), using the standard stars as templates. The results are presented in Table 4. Comparison with the JFK values shows a good agreement. The differences have an rms value of 15 km s^{-1} . Unfortunately the external checking can only be done for a handful of target galaxies. We have found independent determinations for only 5 of the galaxies in our sample, all from Wegner et al (1999). For them, the agreement is also satisfactory since the rms of the differences is the same as for the standard galaxies, 15 km s^{-1} .

2.3. The Measurement of the K-effect and of the spectral features

To measure the spectral characteristics, the spectra were first shifted to zero redshift, using the measured cz values as we mentioned, with the appropriate tasks within IRAF. Then, the K-effect was measured by computing the magnitude in a given band in both the observed and the zero-redshifted spectra. Given the spectral coverage of our data and the redshift of the sources, it was not always possible to compute the K-effect for all the three B, V and Gunn r bands. In fact, the only band for which we have measured the K-effect for all the targets is V. The results are given in Table 4.

In Table 5 we present the average values for every cluster we have observed. Comparing with the values reported by Pence (1976) for E/S0 galaxies, and with the model predictions by Poggianti (1997) for the same type of galaxies, we find a very good agreement. We notice that the scatter of the K-corrections for early type galaxies in clusters is very small, indicating that applying the same correction to all the bright E/S0 galaxies in clusters introduces only small errors.

To measure the 4000 Å break we choose to use bands of 100 Å width on both sides of the feature. This choice is just practical, due to the fact that our spectra do not extend enough into the blue. The data are also collected in Table 4. Even if we cannot directly compare with similar measurements from other authors, we have verified that the range of our values is totally similar to that found by Dressler & Shectman (1988) for similar galaxies in nearby clusters. For the different line indicators we have used the Lick spectral bands as defined in Worthey et al (1994). For reasons we have already indicated, only the most prominent features, Mg_2 , NaD, and the 4000Å break were measured. The results are presented in Table 4.

Let's start considering the Mg_2 strength measurements. First, the internal accuracy can be ascertained from repeated measurements with the same resolution. The rms of the differences for galaxies observed twice in the LRS/20 mode amounts to 0.014, most probably due to the poor S/N of some of the spectra we repeated. Thus, as for the redshift, we consider that the overall quality of the data is definitely better than that figure. Then for the standard galaxies we find a good agreement with JFK values, even if the resolution used is not the same. We notice that the same aperture was used by JFK and here. Except for N1403, for which the Mg_2 value was quoted as uncertain by JFK, as is our own value, due to rather poor S/N, the rms value of the differences is slightly smaller than 0.01 mag, i. e., smaller than for repeated measurements. As we are going to discuss below, this difference mainly reflects the effect of the resolution. Incidentally we notice that the comparison shows up that our results are in the same system as those reported by JFK.

The effect of the resolution on the measured values can be checked comparing the results from LRS/40, LRS/20 and IRS data. Starting with the standard galaxies, for

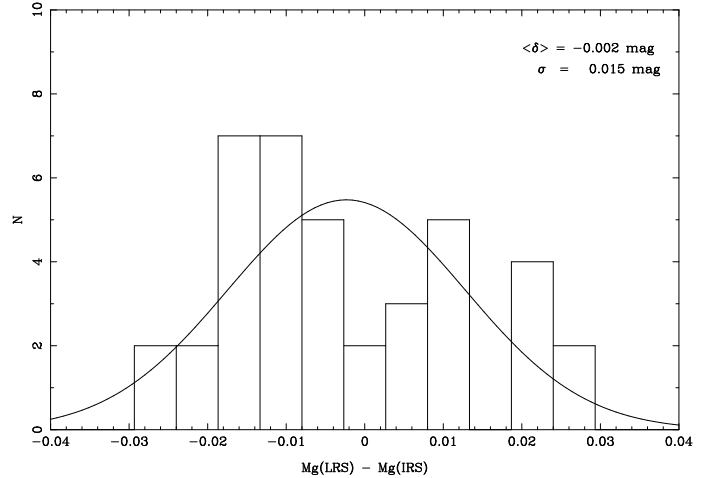


Fig. 2. Distribution of the differences in the Mg_2 values for 42 objects for which both IRS and LRS data are available. The bin size is 0.004. The solid line is the gaussian fit to the binned data

the 8 objects measured in LRS/20 and IRS modes, the average difference amounts to 0.004 mag, with an rms value of 0.014 mag. Much of that scatter is due to a single object, N1395, for which the LRS value is 0.028 mag smaller than the IRS value. Regarding the target galaxies, we have 42 objects for which we could measure the Mg_2 strength from LRS and IRS data. Excluding three grossly discrepant cases (more than 0.03 mag difference), the differences have an average of 0.003 mag, with $\sigma = 0.014$ mag. Their median value amounts to 0.006 mag (see Figure 2).

To test further the effect we have degraded the observed IRS data to produce spectra with the resolution of the LRS/20 and LRS/40 modes. The results are presented in Figure 3. It can be seen that the relations have slopes very close to 1, in particular between LRS/20 and IRS data. The systematic effect can be represented by the relation $Mg_2(\text{IRS}) = Mg_2(\text{LRS}/20) + 0.011$ mag, with a scatter of 0.004 mag. For the LRS/40 data the correction amounts to 0.031 mag, with a scatter of 0.007 mag.

For the other line indicators, we estimate that the errors are of the order of 5% at worst, a figure that is confirmed by the comparison of the values obtained from repeated measurements. The 4000 Å break is a very robust indicator that is not affected by other aspects, whereas an important resolution effect is expected on the NaD values since the Lick bands used to define the index are rather narrow. Given that the wavelength range of the IRS data does not cover the NaD region, and we have not enough data taken in both LRS modes for a sound comparison, we have simply measured the NaD equivalent width for the LRS/20 data degraded to the resolution of the runs 4 and 5, namely 40 Å. The results are plotted in Figure 4. We find that the correction is of the form $EW(\text{LRS}/20) = EW(\text{LRS}/40) + 0.9$ Å. This is the correction we will apply to put all the NaD EW values in the same LRS/20 system.

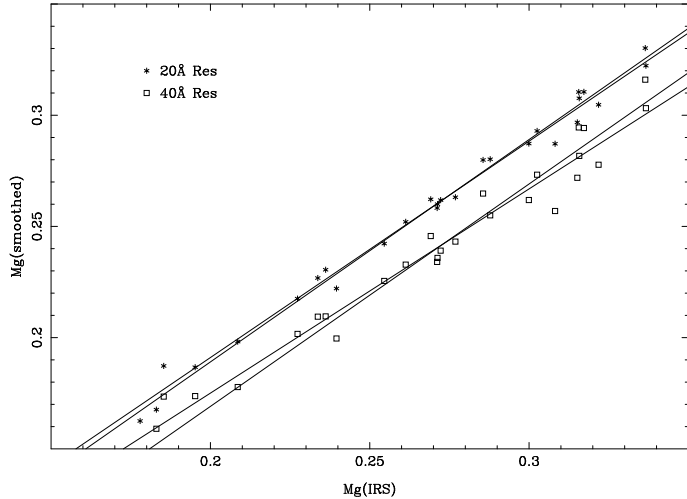


Fig. 3. The relation between the Mg_2 strength values obtained from different resolution data. The plotted lines for the two sets of data are the best fit and the fit with slope = 1 in each case.

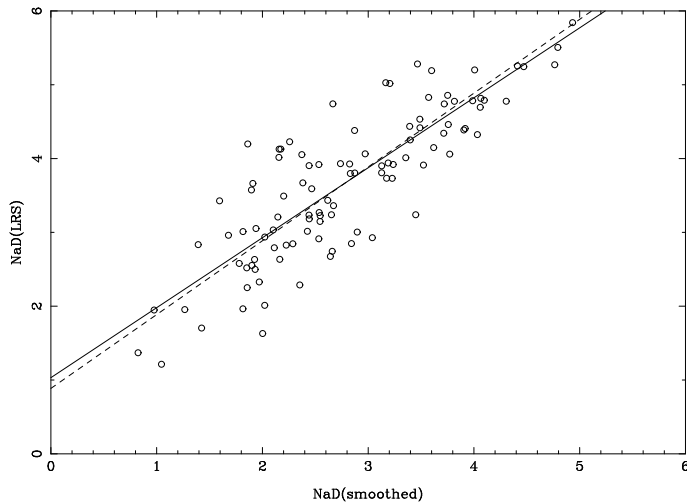


Fig. 4. The EW of the NaD line from real LRS/20 data and from the same spectra degraded to 40 Å resolution. The lines are the best fit and the fit with slope = 1.

2.4. The aperture corrections: The final data

To perform the aperture correction of the Mg_2 index we have followed JFK to transform the observed values to the standard aperture of $1.19h^{-1}$ kpc, corresponding to $3''.4$ at the distance of Coma. Their expression (4) was used to evaluate the correction. As we have already noticed, our data are in a system similar to that of JFK, so we have still to transform our values to put them on the Lick system. This has been done also after JFK, adding 0.011 to our values. Finally, we have not corrected for the velocity dispersion simply because it is not known for most of our galaxies; in any case, for a correction as that proposed by JFK, it would never be bigger than 0.003.

Similarly, an aperture corrections should be applied to the other line indicators. For the NaD equivalent width, given that there are no specific data on its radial gradient,

we decided to apply the same kind of correction as for the Mg_2 index. The final expression for the aperture corrected NaD line EW is given by

$$(EW)_n = W[1 - (r_o/r_n)^{-0.016}] + (EW)_o \times (r_o/r_n)^{-0.016}$$

where the index n(o) stands for aperture corrected (observed) value, and W is the width of the filter used to measure the feature (32.5 Å in the system defined by Worthy et al 1994). The maximum correction, for A98, amounts to 0.60Å, whereas it is of 0.18Å for A119.

For the aperture correction of the 4000Å break we have used the result by Sánchez-Blázquez et al (2001), who have found that the break changes as $-0.20\log(r)$. The maximum correction amounts to 0.11.

The final, corrected values for the redshift, the velocity dispersion and the line indicators are given in Table 6. We have taken the Mg_2 results from the IRS mode when available, correcting the values obtained with LRS data to that resolution following the recipes explicated before, including the correction to put them in the Lick system. For the NaD EW value, we have corrected all the LRS/40 measurements to LRS/20 just adding 0.90Å to take into account the resolution effect as discussed before.

3. General Considerations

3.1. The Redshift of the Clusters

For four clusters, namely A119, A1069, A1983 and A2151, the number of new (or significantly modified) redshift values we can add represents only a small fraction of the total known. There are some cases however, namely A98, A3125, A3330, and DC2103 where that number is significantly increased. Therefore, a new and more precise determination of their redshift and velocity dispersion is possible. We discuss them briefly below. The results are given in Table 5.

We have obtained the redshift for 31 galaxies in the field of A98 (see Table 5), of which 16 are also in Beers et al (1982), or in Zabludoff et al (1990), or in both. Following the preceding discussion on the redshift accuracy of our data, we have adopted our values in all cases when they were also in other references. The redshift distribution of all the galaxies with known cz in the field of A98 is presented in the Figure 5. Considering all the 38 objects with cz in the range between 29500 km s^{-1} and 33000 km s^{-1} , we find for the cluster redshift $cz = 31225 \text{ km s}^{-1}$, with $\sigma = 895 \text{ km s}^{-1}$. We notice that 6 of the 7 foreground galaxies define a group with $cz = 17973 \text{ km s}^{-1}$, and $\sigma = 254 \text{ km s}^{-1}$.

Beers et al (1982) argued that A98 would comprise two spatially and dynamically distinct extensions. With the new data, a total of 11 galaxies are located in the A98N extension, and 25 in A98S. The velocity distribution shown in Figure 5 shows only one peak and is rather smooth. Looking at the two extensions, there is a slight redshift difference between the northern and southern extensions, but is not significant. Therefore, the existence of

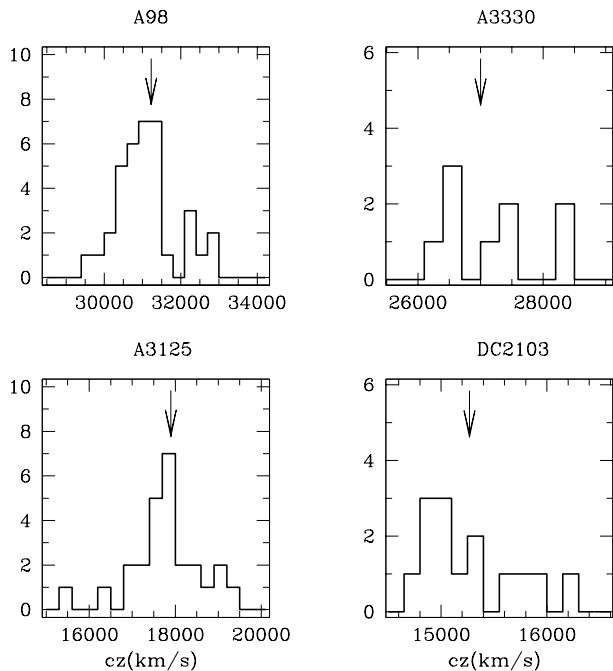


Fig. 5. Distribution of known redshift of galaxies in the clusters A3125, DC2103, A3330 and A98. The arrows indicate the cluster mean cz value as given in the text.

two substructures in cz space is not confirmed with the still scarce data already available.

Considering A3125, Caldwell and Rose (1997) have reported the redshift of 16 galaxies in the field of the cluster. Only five are also in our sample. Together with our measurements, the total amounts now to 31 values. The cz distribution is given in Figure 5. Taking out the 5 outliers (2 fore- and 3 background galaxies), we are left with 26 objects, which define the cluster redshift $cz = 17898 \text{ km s}^{-1}$, with $\sigma = 779 \text{ km s}^{-1}$.

The redshift quoted for A3330 in the compilation by Struble and Rood (1999), $z = 0.0921$, was determined with only two galaxies (Ebeling and Maddox 1997). From the 9 galaxies we have measured, we find $cz = 27000 \text{ km s}^{-1}$, and $\sigma = 695 \text{ km s}^{-1}$, with the distribution plotted in Figure 5.

The situation is similar for the cluster DC2103-39, for which only 3 redshifts were known (Loveday et al 1996). We have measured the redshift of 21 galaxies in the area, of which 6 are foreground and 1 is a background object. For the remaining 14 objects (see Figure 5) we find $cz = 15268 \text{ km s}^{-1}$, with $\sigma = 449 \text{ km s}^{-1}$. All the six foreground objects are at a similar redshift. Five of them are grouped with an average $cz = 9260 \text{ km s}^{-1}$, with $\sigma = 70 \text{ km s}^{-1}$. These galaxies are located in the field we called “a” in Paper I. They could be part of a cluster as more galaxies are visible in that field.

3.2. The range of spectral properties

In Table 5 we also give the range and median values of the K-correction terms and the spectral indicators we have

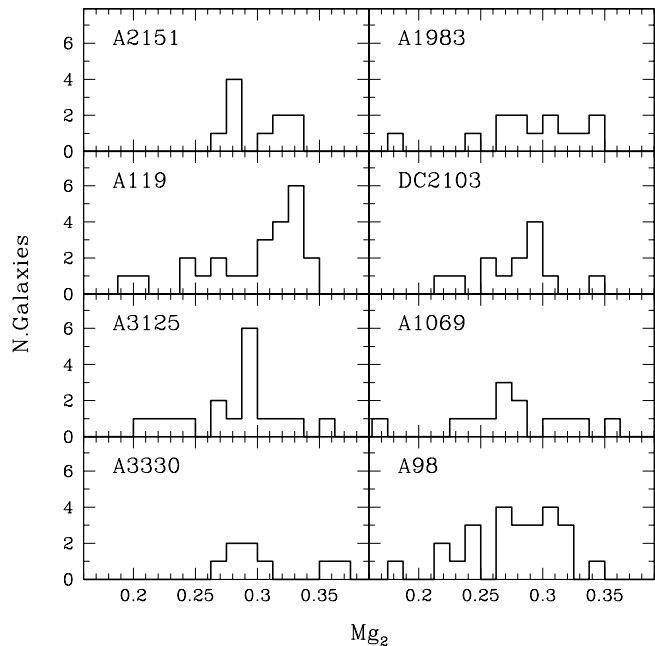


Fig. 6. Distribution of the Mg_2 strength for all the measured galaxies in each cluster.

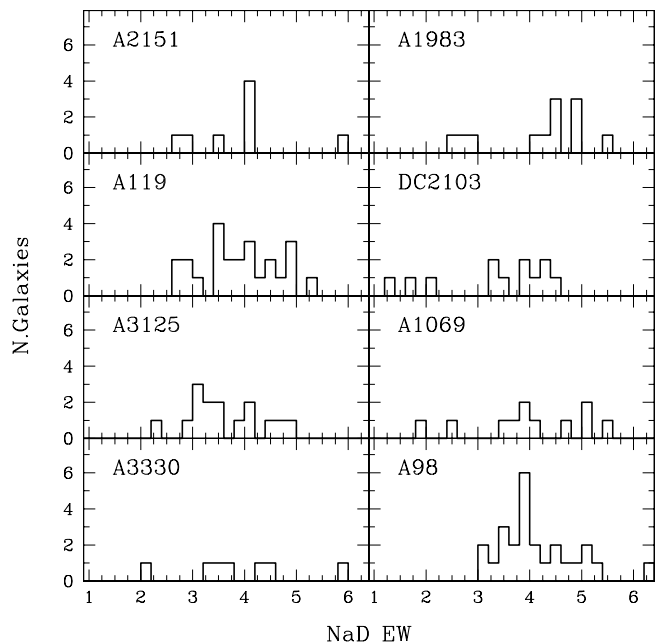


Fig. 7. Distribution of the NaD equivalent width for all the measured galaxies in each cluster.

considered here. The K-correction values, as indicated before, are very similar for all the bright E and S0 galaxies in a given cluster. The average values are very well defined, with a small scatter, and follow the trend with z shown by the data presented by Pence (1976) and with the model prediction by Poggianti (1997) for the same kind of galaxies.

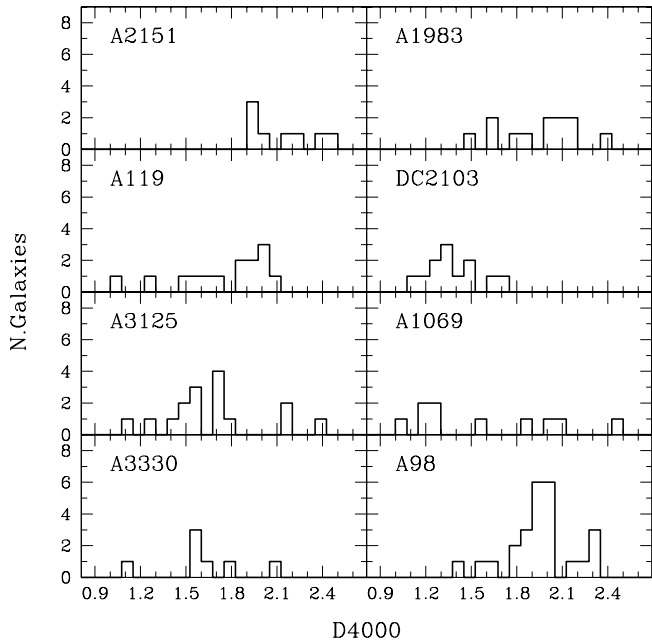


Fig. 8. Distribution of the the 4000Å break line indicator for all the measured galaxies in each cluster.

The Mg_2 values span a rather big range in all the 8 clusters (see Figure 6), in most cases from 0.20 to 0.35. The exceptions are A2151 and A3330 with higher minimum values, what could be due to the small number of objects observed in these clusters. The median values are however different, from 0.269 mag in A1069 to 0.320 mag in A2151. There is no significant trend with cz , finding clusters at similar cz with different median values. The situation is similar for the NaD (Figure 7) equivalent width, with also spans a big range of values in each cluster. The median values are however within 1Å. Finally, for the 4000 Å break (Figure 8), there are differences in the ranges, but could be simply due to the small number of sources. In any case we point out the absence of low D4000 values in A2151, and that of high values in DC2103. We notice that a trend is visible between the NaD and Mg_2 indicator, but with an important scatter (see Figure 9).

3.3. Galaxies with emission lines

The targets we selected were among the brightest cluster galaxies classified as E or S0, so it was not expected to find but a few showing emission lines. Out of a total of 13 of such objects, half are actually foreground objects relative to the cluster under consideration. These are A1069d41, A3125d11, A3125d14, A98F3g4, and DC2103D18. They all have typical HII-like spectra.

The cluster member galaxies with emission lines are the following:

- A119d44. Faint [OIII] λ 5007 detected only in the IRS data

- A119d45. This galaxy presents a spectrum typical of a star forming region
- A3125d160. Faint [OIII] λ 5007 detected only in the IRS data
- A3125d77. It presents strong $H\alpha$ emission, with some structure. There is some indication of high electronic density from the [SII] lines. Neither the [OIII] lines, nor $H\beta$ are visible in our spectrum
- A2151d78. This galaxy (IC1182) is a known peculiar early type object, with a spectrum in the border line between star forming and active galaxies. Its properties have been discussed in Moles et al (2004)
- A98F1g44. It presents all the lines typical of star forming galaxies, from [OII] to [SII]
- A98F1g58. Spectrum typical of an early type galaxy, but with $H\alpha$, [NII] and [SII] clearly visible
- DC2103d18. Faint [OIII] λ 5007 detected only in the IRS data

We notice that all have spectra of star forming regions, and none shows signs of nuclear activity.

4. Summary and Conclusions

We present here LRS and/or IRS for 147 early type galaxies in 8 nearby clusters with $z \leq 0.1$. Data on the redshift, velocity dispersion (for a sub sample), the K-correction, and the most prominent spectral indicators are given.

Comparison of LRS results with IRS and literature data indicate that low resolution spectra can provide accurate values for the redshift (within 65 km s^{-1}), and for the Mg_2 strength (within 0.01 mag). Moreover, since the high and moderate resolution measurements are tightly related, a well defined correction can be applied to obtain all the data in a common base. This means that accurate enough data can be obtained with moderate resolutions, and therefore for galaxies to rather high redshift, an important point for any evolutionary study.

Our data have allowed to give more precise values for the redshift and velocity dispersion of 4 clusters, poorly known to now, namely A98, A3125, A3330, and DC2103 (see Table 5).

Regarding the K-correction terms, our results indicate that it is very similar for all the bright E/S0 galaxies in a given cluster, so the same correction can be applied to all for many studies. Our values are in very good agreement with the data by Pence (1977) and with the model predictions by Poggianti (1997).

Given the short range in redshift of the clusters analyzed here, no trend with z was expected for any of the spectral indicators, as it is found. It is interesting to note, however, that for all three spectral indicators we find a large range of the values for every cluster. It is that physical variance in the spectral properties of the member galaxies what seems to be the most interesting aspect from the present analysis. A trend between the line indicators NaD and Mg_2 is present in our data, in agreement with

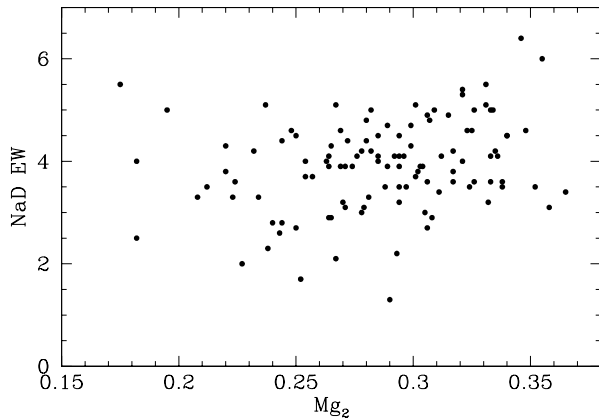


Fig. 9. The Mg_2 strength versus the NaD equivalent length for the galaxies in different clusters

previous results. The 4000Å Break doesn't seem to have a clear relation with the other indicators.

References

- Barbaro, G., & Poggianti, B., 1997, AA, 324, 490
- Beers, T. C., Geller, M. J. & Huchra, J. P., 1982, ApJ, 257, 23
- Beers, T. C., Gebhardt, K., Forman, W., Huchra, J. P., Jones, C., 1991, AJ, 102, 1581
- Bertola, F., Bettoni, D., Rusconi, L. & Sedmak, G., 1984, AJ, 89, 356
- Bica, E. L. D., & Alloin, D., 1986, A&A, 166, 83
- Bica, E. L. D., Pastoriza, M., Maia, M., da Silva, L., & Dottori, H., 1991, AJ, 102, 1072
- Bureau, M. Mould, J. R., & Staveley-Smith, L., 1996, ApJ, 463, 60
- Burstein, D., Faber, S. M., Gaskell, C. M., & Krumm, N., 1984, ApJ, 287, 586
- Caldwell, N. & Rose, J. A., 1997, AJ, 113, 492
- da Costa, L. N., Pellegrini, P. S., Davis, M., Meiksin, A., Sargent, W. L. W. & Tonry, J. L., 1991, ApJS, 75, 935
- Davoust, E. & Considere, S., 1995, A&AS, 110, 19D
- van Dokkum, P. G., & Franx, M., 1996, MNRAS, 281, 985
- Dressler, A., 1980, ApJS, 42, 565
- Dressler, A., & Shectman, S. A., 1987, AJ, 94, 899
- Dressler, A., & Shectman, S. A., 1988, AJ, 95, 284
- Ebeling, H., & Maddox, S. J., 1995, MNRAS, 275, 1155
- Falco, E. E., Kurtz, M. J., Geller, M. J., Huchra, J. P., Berlind, P., Mink, D. J., Tokarz, S. P., & Elwell, B., 1999, PASP, 111, 438
- Fasano, G., Poggianti, B. M., Couch, W. J., Bettoni, D., Kjærgaard, P. & Moles, M., 2000, ApJ, 542, 673
- Fasano, G., Bettoni, D., D'Onofrio, M., Kjærgaard, P. & Moles, M., 2002, A&A, 387, 26 (Paper I)
- Fasano, G. et al. 2006, A&A, 445, 805
- Fouqué, P., Gourgoulhon, E., Chamaraux, P. & Paturel, G., 1992, A&AS, 93, 211
- Gorgas, J., Cardiel, N., Pedraz, S., & González, J. J., 1999, A&AS, 139, 29
- Graham, A. W., Colless, M. M., Busarello, G., Zaggia, S., & Longo, G., 1998, A&AS, 133, 325
- Hamilton, D., 1985, ApJ, 297, 371
- Huchra, J. P.; Vogeley, M. S.; Geller, M. J., 1999, ApJS, 121, 287
- Jørgensen, I., Franx, M., & Kjærgaard, P., 1996, MNRAS, 280, 167 (JFK)
- Katgert, P., Mazure, A., Perea, J., den Hartog, R., Moles, M., Le Fèvre, O., Dubath, P.P., Focardi, P., Rhee, G., Jones, B., Escalera, E., Biviano, A., Gerbal, D., & Giuricin, G., 1996, AA, 310, 8
- Katgert, P., Mazure, A., den Hartog, R., Adami, C., Biviano, A., & Perea, J., 1998, A&AS, 129, 399
- Kimble, R. A., Davidsen, A. F., Sandage, A. R., 1989, ApJSS, 157, 237
- Kjærgaard, P., Jørgensen, I., & Moles, M., 1993, ApJ, 418, 617 (KJM)
- Lauberts, A., & Valentjin, E. A., 1989, The Surface Photometry Catalogue of the ESO-Uppsala Galaxies, Garching bei München, ESO
- Loveday, J., Efstathiou, G., Maddox, S. J. & Peterson, B. A., 1996, ApJ, 468, 1
- Moles, M., Campos, A., Kjaegaard, P., Fasano, G., & Bettoni, D., 1998, ApJ Letters, 495, L31
- Moles, M., Bettoni, Fasano, G., Kjaegaard, P., Varela, J. & Milvang-Jensen, B. 2004, A&A, 418, 495
- Paturel, G., Petit, C., Prugniel, P., Theureau, G., Rousseau, J., Brouty, M., Dubois, P., Cambresy, L., 2003, A&A, 412, 45
- Pence, W., 1976, ApJ, 203, 39
- Poggianti, B. M., & Barbaro, G., 1997, A&A, 325, 1025
- Poggianti, B. M., 1997, A&AS, 122, 399
- Postman, M. & Lauer, T. R., 1995ApJ, 440, 28
- Snchez-Blzquez, P., Gorgas, J., Cardiel, N., Pedraz, S., Cenarro, A. J., Bruzual, G., 2001, ApSSS, 277, 351
- Sargent, W. L. W., Schechter, P. L., Boksenberg, A. & Shortridge, K. 1977, ApJ, 212, 326
- Simien, F., & Prugniel, P., 1997, AASS, 126, 519
- Smith, R. J., Lucey, J. R., Hudson, M. J., Schlegel, D. J., & Davies, R. L. 2000, MNRAS, 313, 469
- Struble, M. F., & Rood, H. J., 1999, ApJS, 125, 35
- de Vaucouleurs, G., de Vaucouleurs, A., Corwin Jr., H. G., Buta, R. J., Paturel, G., Fouqué, P., 1991, Third Reference Catalogue of Bright Galaxies, RC3
- Wegner, G., Colless, M., Saglia, R. P., McMahon, R. K., Davies, R. L., Burstein, D., & Bagglely, G., 1999, MNRAS, 305, 259
- Worthy, G., Faber, S. M., González, J., & Burstein, D., 1994, ApJS, 94, 687
- Zabludoff, A. I., Huchra, J. P., & Geller, M. J., 1990, ApJS, 74, 1
- Zabludoff, A. I.; Geller, M. J.; Huchra, J. P.; Vogeley, M. S., 1993, AJ, 106, 1273

Table 3. Galaxies not included in Dressler (1980)

Galaxy	$\alpha(2000)$	$\delta(2000)$	<i>Spectrum id.</i>
<i>Abell 98</i>			
2MASXJ00463567 + 2029428	00 : 46 : 35.7	+20 : 29 : 42	F1g20
2MASXJ00463524 + 2030108	00 : 46 : 35.3	+20 : 30 : 11	F1g22
A98 : [BGH82]320	00 : 46 : 24.7	+20 : 30 : 07	F1g30
2MASXJ00462380 + 2030006	00 : 46 : 23.9	+20 : 30 : 00	F1g31
2MASXJ00462059 + 2029076	00 : 46 : 20.7	+20 : 29 : 07	F1g38
2MASXJ00461931 + 2029416	00 : 46 : 19.4	+20 : 29 : 41	F1g43
A98 : [BGH82]311	00 : 46 : 16.0	+20 : 30 : 19	F1g44
2MASXJ00463702 + 2026068	00 : 46 : 37.1	+20 : 26 : 06	F1g58
2MASXJ00462586 + 2027326	00 : 46 : 25.9	+20 : 27 : 32	F1g65
3C021	00 : 46 : 29.4	+20 : 28 : 04	F1g76
2MASXJ00463318 + 2027518	00 : 46 : 33.2	+20 : 27 : 51	F1g77
2MASXJ00463183 + 2028118	00 : 46 : 31.9	+20 : 28 : 11	F1g80
2MASXJ00463624 + 2028268	00 : 46 : 36.3	+20 : 28 : 26	F1g88
2MASXJ00463624 + 2028268	00 : 46 : 08.5	+20 : 28 : 50	F2g01
2MASXJ00460743 + 2028486	00 : 46 : 07.5	+20 : 28 : 48	F2g02
A98 : [PBL2000]0264	00 : 46 : 04.8	+20 : 28 : 27	F2g03
2MASXJ00455043 + 2027487	00 : 45 : 50.5	+20 : 27 : 49	F2g05
2MASXJ00455043 + 2027487	00 : 45 : 50.4	+20 : 29 : 08	F2g07A
2MASXJ00455008 + 2029097	00 : 45 : 50.2	+20 : 29 : 09	F2g07B
2MASXJ00460209 + 2030516	00 : 46 : 02.2	+20 : 30 : 50	F2g09
2MASXJ00461355 + 2034516	00 : 46 : 13.6	+20 : 34 : 51	F3g01
2MASXJ00460400 + 2034516	00 : 46 : 04.0	+20 : 34 : 51	F3g02
A98 : [BGH82]182	00 : 45 : 59.8	+20 : 35 : 09	F3g03
NPM1G + 20.0024	00 : 45 : 52.9	+20 : 35 : 13	F3g04
A98 : [PBL2000]376	00 : 45 : 57.5	+20 : 36 : 56	F3g05
2MASXJ00460400 + 2034516	00 : 46 : 04.5	+20 : 36 : 45	F3g07
A98 : [PBL2000]269	00 : 46 : 17.1	+20 : 23 : 44	F10g5
2MASXJ00461469 + 2023426	00 : 46 : 14.7	+20 : 23 : 42	F10g6
2MASXJ00462849 + 2023488	00 : 46 : 28.5	+20 : 23 : 48	F10g7
2MASXJ00463390 + 2023548	00 : 46 : 34.0	+20 : 23 : 55	F10g8
2MASXJ00463852 + 2022538	00 : 46 : 38.6	+20 : 22 : 53	F10g9
<i>Abell 3330</i>			
2MASXJ05145263 - 4859071	05 : 14 : 52.5	-48 : 59 : 07	g21
2MASXJ05145588 - 4859121	05 : 14 : 55.7	-48 : 59 : 12	g22
2MASXJ05150675 - 4901321	05 : 15 : 06.6	-49 : 01 : 33	g5
2MASXJ05150726 - 4902261	05 : 15 : 07.2	-49 : 02 : 27	g6
APMUKS(BJ)B051342.65 - 490606.2	05 : 15 : 00.7	-49 : 02 : 48	g7
FAIRALL0790	05 : 14 : 39.4	-49 : 03 : 29	g1
2MASXJ05143494 - 4905153	05 : 14 : 34.9	-49 : 05 : 15	g2
2MASXJ05150574 - 4905461	05 : 15 : 05.6	-49 : 05 : 47	g4
2MASXJ05142945 - 4905534	05 : 14 : 29.3	-49 : 05 : 54	g3

Table 4: continued

Galaxy	LRS data										IRS data					Comments
	cz	Q	Refs	k_B	k_V	k_r	D4000	Mg ₂	NaD	Run	cz	ϵ	σ	ϵ	Mg ₂	
D11	8682 ^o	1	1,8	–	.02	.03	–	–	–	1	–	–	–	–	–	EL
D14	15532	1	–	–	.15	.12	–	–	–	1	–	–	–	–	–	EL
D46	17900	3	9	–	.13	.08	1.64	.270	4.4	1	17830	38	253	24	.276	$\Delta V = 50$
D47	17816	2	9	–	.13	.09	1.76	.241	3.8	1	17745	31	299	42	.269	–
D48	17346	1	9	–	.12	.08	2.14	.189	3.0	1	–	–	–	–	–	–
D51	18790	1	–	–	.14	.09	2.08	.282	4.3	1, 2	18845	36	213	46	.300	–
D60	17587	1	9	–	.13	.09	1.54	.255	3.6	1	17478	45	291	59	.281	–
D77	17440	2	–	–	.11	.07	–	–	–	1	17298	70	261	67	–	EL
D88	17675	2	–	–	.14	.09	1.06	.332	4.7	1	17693	71	332	85	.310	$\Delta V = 189$
D93	17485	1	9	–	.11	.07	1.22	.259	2.9	2	17621	35	287	77	.271	–
D95	–	–	–	–	–	–	–	–	–	–	17866	61	335	34	.263	$\Delta V = 73$
D96	17702	3	9	–	.13	.10	2.33	.198	2.0	1	17652	48	239	22	.215	–
D103	17786	1	–	–	.13	–	1.54	.177	3.0	2	17766	49	288	11	.185	–
D104	18099	1	–	–	.14	.09	1.67	.237	2.8	1	–	–	–	–	–	–
D129	18890	1	9	–	.13	.09	1.47	.231	2.6	1	–	–	–	–	–	–
D130	19112	2	9	–	.13	.09	1.53	.281	3.2	1	19049	27	236	25	.271	–
D140	18917	2	9	–	.15	.10	1.64	.211	3.9	1	18945	39	212	5	.209	–
D160	18361	1	9	–	.15	.10	1.39	.263	3.2	1	18459	46	262	61	–	EL
D161	18115	2	–	–	.14	.10	1.68	.315	2.8	1, 2	17964	79	328	35	.336	–
Abell 3330																
G1	27522	2	–	–	.10	–	1.54	.244	4.0	1	–	–	–	–	–	–
G2	26446	2	–	–	.10	–	1.00	.226	1.6	1	–	–	–	–	–	–
G3	27358	2	–	–	.15	–	2.66	.260	3.2	1	–	–	–	–	–	–
G4	26586	3	–	–	.13	–	1.97	.242	–	1	–	–	–	–	–	–
G5	28262	1	–	–	.17	–	1.45	.314	5.5	1	–	–	–	–	–	–
G6	27140	1	–	–	.14	–	1.68	.258	3.8	1	–	–	–	–	–	–
G7	26222	1	–	–	.11	–	–	–	–	1	–	–	–	–	–	EL
G21	26463	1	–	–	.19	–	1.50	.324	2.9	1	–	–	–	–	–	–
G22	28251	1	–	–	.20	–	1.44	.247	3.0	1	–	–	–	–	–	–
Abell 1069																
D3	19336	1	–	–	.10	.07	1.16	.232	4.8	1	–	–	–	–	–	–
D9	19478	3	–	–	.11	.07	2.44	.234	3.6	1	–	–	–	–	–	–
D12	16624	2	7	–	.08	.07	1.66	.253	2.3	1	–	–	–	–	–	–
D14	16656	1	–	–	.08	.07	1.38	.275	3.6	1	–	–	–	–	–	–
D15	19737	1	1,7	–	.10	.07	1.51	.235	3.9	1,6	19709	23	239	9	.292	–
D16	20110	4	1	–	.09	.07	1.00	.140	5.2	1	–	–	–	–	–	–
D19	18030	1	1,7	–	.10	.08	1.10	.224	3.7	1,6	18040	31	220	11	.261	–
D21	19817	2	1,7	–	.11	.06	1.20	.319	3.2	1,6	19345	31	357	9	.328	–
D25	20331	1	1,7	–	.09	.04	1.82	.212	2.3	1,6	20287	19	275	7	.219	–
D29	20051	1	1,7	–	.10	.07	2.00	.259	4.5	1,6	20067	17	236	7	.283	–
D30	20430	1	1	–	.08	.06	1.22	.219	3.4	1	–	–	–	–	–	–
D38	19329	2	–	–	.11	.08	–	.244	–	1,6	19432	19	295	7	–	–
D39	19729	3	–	–	.09	.07	–	.192	1.7	1	–	–	–	–	–	–
D41	11644	1	–	–	–	–	–	–	–	1	–	–	–	–	–	EL
D46	19700	2	–	–	.09	.05	1.97	.248	4.8	1,6	19653	19	231	8	.307	–
D47	–	–	–	–	–	–	–	–	–	6	18931	14	149	10	.250	–
Abell 1983																
D6	17547	1	10	–	–	–	1.66	.186	2.0	3	–	–	–	–	–	–
D10	13156	1	10	–	.07	–	1.60	.303	5.3	3	–	–	–	–	–	–
D15	13589	1	10	–	.07	–	2.11	.292	4.3	3,6	13676	20	323	7	.323	–
D23	12782	1	10	–	.05	–	1.46	.154	2.3	3	–	–	–	–	–	–
D24	13504	1	10	–	.07	–	1.59	.241	4.4	3	–	–	–	–	–	–
D26	17822	1	10	–	–	–	1.90	.294	4.4	3	–	–	–	–	–	–
D28	6251	1	10	–	.04	–	1.59	.180	2.0	3	–	–	–	–	–	–
D35	13659	1	10	–	.08	–	2.36	.237	4.1	3	–	–	–	–	–	–
D46	13532	1	10	–	.07	–	2.15	.280	2.7	3	–	–	–	–	–	–
D54	13167	2	7	–	.07	–	1.79	.297	4.7	3,6	12979	14	232	7	.298	–
D56	13481	1	10	–	.07	–	2.04	.285	4.8	3,6	13583	20	198	9	.265	–
D58	13606	1	11	–	.07	–	2.03	.212	2.6	3	–	–	–	–	–	–
D77	–	–	–	–	–	–	–	–	–	6	13844	15	215	8	.266	–
D78	13781	1	7	–	.06	–	1.85	.306	3.9	3,6	13639	15	212	8	.277	–
D84	13894	1	11	–	.08	–	1.96	.281	4.8	3	–	–	–	–	–	–
D105	13310	1	10	–	.06	–	1.98	.264	4.3	3,6	13387	20	323	7	.323	–
Abell 2151																
D4	9986	3	10	.18	.06	–	1.91	.219	1.9	4	–	–	–	–	–	–
D7	10055	1	2	.20	.07	–	2.23	.290	3.2	4	–	–	–	–	–	–
D9	10248	1	10	.18	.06	–	1.90	.261	1.7	4	–	–	–	–	–	–
D15	9966	1	10	.19	.06	–	1.96	.281	2.6	4	–	–	–	–	–	–
D40	10330	1	12	.19	.04	–	2.12	.268	3.1	4,6	10050	15	230	7	.271	–
D62	9338	1	2	.18	.06	–	2.36	.233	3.2	4	–	–	–	–	–	–
D63	10830	1	10	.21	.07	–	2.43	.281	3.1	4,6	10455	16	195	9	.262	–
D64	10432	2	10	.21	.07	–	1.97	–	5.0	4	–	–	–	–	–	–
D65	–	–	–	–	–	–	–	–	–	6	10426	13	291	6	.305	–
D66	–	–	–	–	–	–	–	–	–	6	9643	9	186	6	.270	–
D78	10262	1	–	.13	.05	–	–	–	–	4	–	–	–	–	–	EL
D134	–	–	–	–	–	–	–	–	–	6	11074	50	318	11	.302	–

Table 4: continued

Galaxy	LRS data										IRS data					Comments
	cz	Q	Refs	k_B	k_V	k_r	D4000	Mg ₂	NaD	Run	cz	ϵ	σ	ϵ	Mg ₂	
DC 2103-39																
D3	16114	1	–	.26	.13	.03	1.33	.268	4.2	2	16152	35	185	27	.272	$\Delta V = 150$
D14	9374	1	–	.13	.05	.02	1.28	.329	4.9	2	9343	40	332	58	.327	–
D15	15034	1	–	.23	.09	.04	1.32	.335	3.2	2	15038	39	237	30	.316	$\Delta V = 103$
D18	9319	2	–	–	.05	.03	–	–	–	2	9208	30	137	38	–	EL, $\Delta V = 122$
D20	9287	1	–	.11	.04	.02	1.00	.185	1.8	2	9353	19	154	38	.191	–
D21	9161	1	–	.15	.06	.03	1.49	.229	2.5	2	9400	31	242	64	.218	$\Delta V = 91$
D23	9279	1	–	.13	.07	.03	1.25	.273	2.6	2	9245	62	260	52	.244	$\Delta V = 270$
D38	15820	1	–	.22	.08	.04	1.60	.232	3.0	2	15742	52	275	47	.212	–
D39	15869	3	–	.26	.09	.04	1.19	.252	1.0	2	15892	51	313	23	.268	–
D40	15060	1	–	.22	.08	.04	1.47	.249	3.9	2	14992	33	223	17	.260	–
D42	14719	1	–	.20	.10	–	1.47	.240	3.6	2	14700	24	206	71	.249	–
D53	26506	1	–	–	.13	–	1.97	.287	3.7	2	26558	60	316	23	–	–
D60	15635	2	–	.22	.11	.05	1.25	.224	3.7	2	15626	32	177	58	.232	–
D61	15369	2	–	.20	.10	.04	1.33	.278	3.1	2	15326	33	200	69	–	–
D62	15149	1	–	–	.07	.03	1.07	.227	1.4	2	15079	23	176	17	.230	–
D63	15003	2	–	–	.08	.03	1.16	–	1.9	2	14937	23	147	24	.271	–
D66	9527	2	–	–	.04	.02	1.18	.166	0.8	2	9581	39	235	23	.177	–
D71	14836	1	–	–	.08	.04	1.37	.249	4.1	2	14832	44	207	33	.258	–
D73	–	–	–	–	–	–	–	–	–	–	14940	38	260	17	.276	–
D76	15230	3	–	.20	.08	.03	1.66	.187	4.0	2	–	–	–	–	–	–
D102	–	–	–	–	–	–	–	–	–	–	15324	39	207	55	–	$\Delta V = 92$

References for the redshift. (A) Standard Galaxies: a, JFK; b, Smith et al (2000); c, Graham et al (1998); d, de Vaucouleurs et al (1991, RC3); e, Bureau et al (1996); f, Lauberts & Valentijn (1989, ESO-Uppsala Catalog); g, Simien and Prugniel (1997); h: da Costa et al. (1991). (B) Cluster Galaxies. 1: Katgert et al (1998, ENACS Catalog); 2, de Vaucouleurs et al (1991, RC3); 3, Huchra et al (1999, CfA Catalog); 4, Zabludoff et al (1993); 5, Paturel et al (2003, LEDA Catalogue); 6, Postman & Lauer (1995); 7, Beers et al (1991); 8, Lauberts & Valentijn (1989, ESO-Uppsala Catalog); 9, Caldwell & Rose (1997); 10, Dressler & Shectman (1988); 11, Zabludoff et al (1990); 12, Davoust & Considere (1995) *Notes on discrepant redshift results*.

- a. In agreement with B82, but 394 km s⁻¹ higher than in Zabludoff et al (1990)
- b. 634 km s⁻¹ higher than in Z90
- c. Our value, determined from the emission lines, agrees with Z90, but it is 735 km s⁻¹ lower than in Beers et al (1982)
- d. Our value agrees with Z90, and is 9826 km s⁻¹ higher than in Beers et al (1982)
- e. The redshift we find for this galaxy is 368 km s⁻¹ higher than in Beers et al (1982), but grossly discrepant with Zabludoff et al (1990)
- f. Observed in LRS and IRS modes with concordant results. Our LRS value is 337 km s⁻¹ higher than in the ENACS Catalogue.
- g. Observed in LRS and IRS modes with concordant results. Our LRS value is 1038 km s⁻¹ lower than in the ENACS Catalogue, and very close to that reported by Fouqué et al (1992)
- h. Observed twice in LRS mode and in IRS mode, with concordant results. Our LRS value is 1330 km s⁻¹ lower than in the ENACS Catalogue.
- i. Observed in LRS and IRS modes with concordant results. Our LRS value is 1357 km s⁻¹ lower than in the ENACS Catalogue. The redshift reported by Falco et al (1999) is very close to our value, whereas that reported by Fouqué et al (1992) does not agree with any of previous determinations.
- j. Observed in LRS and IRS modes with concordant results. Our LRS value is 1226 km s⁻¹ higher than in the ENACS Catalogue.
- k. Observed in LRS and IRS modes with concordant results. Our LRS value is 1210 km s⁻¹ lower than in the ENACS Catalogue. The redshift reported by Fouqué et al (1992) is very close to our value.
- l. Observed in LRS and IRS modes with concordant results. Our LRS value is 2086 km s⁻¹ higher than in the ENACS Catalogue.
- m. Observed in LRS and IRS modes with concordant results. Our LRS value is 2819 km s⁻¹ higher than in the ENACS Catalogue.
- n. Observed in LRS and IRS modes with concordant results. Our LRS value is 5393 km s⁻¹ lower than in the ENACS Catalogue.
- o. Our redshift is 9478 km s⁻¹ lower than in the ENACS Catalogue, that is in agreement with the redshift given in the ESO-Uppsala catalog. Our value is from the detected emission lines.

Table 5. Average values for the clusters

Cluster	cz	σ	Mg ₂	NaD	D4000	k_B	k_V	k_r
A98	31225	895	0.182-0.346 (0.280)	3.1-6.4 (4.0)	1.45-2.34 (1.95)	0.52 (0.06)	–	–
A119	13260	773	0.195-0.348 (0.303)	2.7-5.3 (4.1)	1.03-2.06 (1.84)	0.22 (0.03)	0.07 (0.02)	0.03 (0.01)
A3125	17898	779	0.208-0.358 (0.294)	2.3-5.0 (3.5)	1.12-2.39 (1.64)	–	0.13 (0.01)	0.09 (0.01)
A3330	27000	695	0.267-0.365 (0.299)	2.1-6.0 (4.0)	1.09-2.75 (1.63)	–	0.14 (0.03)	–
A1069 ^a	19671	659	0.175-0.354 (0.269)	2.0-5.5 (3.9)	1.06-2.50 (1.44)	–	0.10 (0.01)	0.07 (0.01)
A1983	13080	948	0.182-0.334 (0.309)	2.5-5.5 (4.5)	1.49-2.39 (1.99)	–	0.07 (0.01)	–
A2151	10980	716	0.264-0.415 (0.320)	2.7-6.0 (4.1)	1.91-2.44 (2.06)	0.19 (0.01)	0.06 (0.01)	–
DC2103	15268	449	0.220-0.338 (0.282)	1.3-4.5 (3.7)	1.11-1.70 (1.37)	0.22 (0.02)	0.09 (0.02)	0.04 (0.01)

The values of cz and σ for A98, A3125, A3330, and DC2103 are from the present work. For the other clusters they have been taken from Struble and Rood (1999).

For the spectral line indicators we give the range and the median value (in parenthesis). For the K-correction only the median value is given.

Table 6: The adopted, fully corrected, redshift and spectral indicators

Galaxy	cz	D4000	NaD	Mg ₂	log σ
Abell 98					
F1g20	32104	2.02	3.2	.270	–
F1g22	30852	2.34	4.5	.250	–
F1g30	31358	1.92	4.6	.248	–
F1g31	29984	2.33	3.6	.306	–
F1g38	31021	2.22	3.9	.294	–
F1g43	33099	2.29	3.1	.279	–
F1g44	30605	–	–	–	–
F1g58	30654	–	–	–	–
F1g65	31049	2.18	4.0	.321	–
F1g76	30898	2.03	6.4	.346	–
F1g77	42272	1.66	4.6	.242	–
F1g80	32312	2.01	3.9	.289	–
F1g88	32122	2.03	5.4	.321	–
F2g1	30484	1.55	4.0	.182	–
F2g1A	31475	2.02	4.1	.264	–
F2g3	31605	1.93	4.4	.244	–
F2g5	31100	1.95	3.8	.302	–
F2g7A	31005	1.95	4.9	.306	–
F2g7B	30510	1.78	3.3	.281	–
F2g9	30151	2.02	5.1	.301	–
F3g1	17871	1.93	4.1	.332	–
F3g2	30169	1.86	4.1	.296	–
F3g3	31164	1.86	4.8	.280	–
F3g4	10988	–	–	–	–
F3g5	30343	1.45	3.8	.220	–
F3g7	31284	1.95	3.5	.324	–
F10g5	35868	1.92	3.2	.268	–
F10g6	31037	1.97	3.9	.274	–
F10g7	30370	1.78	5.1	.237	–
F10g8	32834	1.86	3.9	.264	–
F10g9	31094	1.63	3.6	.224	–
Abell 119					
D26	13462	1.90	4.0	.263	2.238
D36	13958	1.96	3.8	.317	–
D37	12872	–	5.0	.326	2.380
D38	12591	1.91	3.6	.317	–
D41	12342	–	4.1	.333	2.238
D44	13081	–	3.2	.332	2.303
D45	12660	–	–	–	–
D47	14628	1.30	3.0	.278	2.288
D49	13733	1.65	2.7	.250	2.464
D51	12540	1.99	5.3	.321	–
D52	13447	1.84	4.6	.348	2.422
D60	11565	–	4.3	.319	2.520
D62	13077	–	3.6	.338	2.207
D66	13356	–	5.0	.334	2.431
D68	12225	–	4.6	.325	2.342
D74	12647	–	3.7	.257	2.396
D75	11560	–	2.9	.273	2.223
D93	11705	–	4.7	.289	2.322
D94	12553	2.06	4.1	.312	–
D99	13540	–	3.0	.305	2.428

Table 6: continued

Galaxy	cz	D4000	NaD	Mg ₂	log σ
D102	13258	2.03	5.0	.195	2.292
D105	13350	1.70	3.9	.303	2.496
D107	13085	1.03	3.6	.333	2.196
D109	13021	–	3.5	.212	2.350
D111	12585	1.58	4.4	.272	2.396
D112	14650	1.46	2.8	.244	2.340
D114	13375	2.03	4.1	.336	2.107
Abel 3125					
D9	18508	1.50	–	.295	–
D11	8682	–	–	–	–
D14	15532	–	–	–	–
D46	17830	1.69	4.7	.299	2.403
D47	17745	1.81	4.1	.292	2.476
D48	17346	2.19	3.3	.223	–
D51	18845	2.13	4.6	.323	2.328
D60	17478	1.59	3.9	.304	2.464
D77	17298	–	–	–	2.417
D88	17693	1.11	5.0	.333	2.521
D93	17621	1.27	3.2	.294	2.458
D95	17866	–	–	.287	2.525
D96	17652	2.38	2.3	.238	2.378
D103	17766	1.59	3.3	.208	2.459
D104	18099	1.72	3.1	.271	–
D129	18890	1.52	2.9	.265	–
D130	19049	1.58	3.5	.294	2.373
D140	18945	1.69	4.2	.232	2.326
D160	18459	1.44	3.5	.297	2.418
D161	17964	1.73	3.1	.358	2.516
Abel 3330					
g1	27522	1.63	4.5	.285	–
g2	26446	1.09	2.1	.267	–
g3	27358	2.75	3.7	.301	–
g4	26586	2.06	–	.283	–
g5	28262	1.54	6.0	.355	–
g6	27140	1.77	4.3	.299	–
g7	26222	–	–	–	–
g21	26463	1.59	3.4	.365	–
g22	28251	1.53	3.5	.288	–
Abell 1069					
D3	19336	1.22	5.1	.267	–
D9	19478	2.50	3.9	.269	–
D12	16624	1.72	2.6	.288	–
D14	16656	1.44	3.9	.310	–
D15	19709	1.57	4.2	.317	2.378
D16	20110	1.06	5.5	.175	–
D19	18040	1.16	4.0	.285	2.342
D21	19345	1.26	3.5	.352	2.553
D25	20247	1.88	2.6	.243	2.439
D29	20067	2.06	4.8	.307	2.373
D30	20430	1.28	3.7	.254	–
D38	19432	–	–	.279	2.470
D39	19729	–	2.0	.227	–
D41	11644	–	–	–	–

Table 6: continued

Galaxy	cz	D4000	NaD	Mg ₂	log σ
D46	19653	2.03	5.1	.331	2.364
D47	18931	–	–	.274	2.173
Abell 1983					
D6	17547	1.69	2.2	.214	–
D10	13156	1.63	5.5	.331	–
D15	13676	2.14	4.5	.340	2.509
D23	12782	1.49	2.5	.182	–
D24	13504	1.62	4.6	.269	–
D26	17822	1.93	4.6	.322	–
D28	6251	1.60	2.1	.205	–
D35	13659	2.39	4.3	.265	–
D46	13532	2.18	2.9	.308	–
D54	12979	1.82	4.9	.315	2.365
D56	13583	2.07	5.0	.282	2.297
D58	13606	2.06	2.8	.240	–
D77	13844	–	–	.283	2.332
D78	13639	1.88	4.1	.294	2.326
D84	13894	1.99	5.0	.309	–
D105	13387	2.01	4.5	.340	2.509
Abel 2151					
D4	9986	1.92	2.9	.264	–
D7	10055	2.24	4.2	.335	–
D9	10248	1.91	2.7	.306	–
D15	9966	1.97	3.6	.326	–
D40	10050	2.13	4.1	.285	2.362
D62	9338	2.37	4.2	.278	–
D63	10455	2.44	4.1	.276	2.290
D64	10432	1.98	6.0	–	–
D65	10426	–	–	.319	2.464
D66	9643	–	–	.284	2.270
D78	10262	–	–	–	–
D134	11074	–	–	0.316	2.502
DC2103-39					
D3	16152	1.37	4.5	.294	2.267
D14	9343	1.31	5.0	.342	2.521
D15	15038	1.36	3.5	.338	2.375
D18	9208	–	–	–	2.137
D20	9353	1.01	1.9	.206	2.188
D21	9400	1.50	2.6	.233	2.384
D23	9245	1.26	2.7	.259	2.415
D38	15742	1.64	3.3	.234	2.439
D39	15892	1.23	1.3	.290	2.496
D40	14992	1.51	4.2	.282	2.348
D42	14700	1.51	3.9	.271	2.314
D53	26558	2.06	4.3	.348	2.500
D60	15626	1.29	4.0	.254	2.248
D61	15326	1.37	3.4	.311	2.301
D62	15079	1.11	1.7	.252	2.246
D63	14937	1.20	2.2	.293	2.167
D66	9581	1.19	–	.192	2.371
D71	14832	1.41	4.4	.280	2.316
D73	14940	–	–	.298	2.415
D76	15230	1.70	4.3	.220	–

Table 6: continued

Galaxy	cz	D4000	NaD	Mg ₂	log σ
D102	15324	–	–	–	2.316